

Fractal Dynamics in Chaotic Quantum Transport

V. Kotimäki,¹ E. Räsänen,^{2,1,3,*} H. Hennig,³ and E. J. Heller³

¹*Nanoscience Center, Department of Physics, University of Jyväskylä, FI-40014 Jyväskylä, Finland*

²*Department of Physics, Tampere University of Technology, FI-33101 Tampere, Finland*

³*Physics Department, Harvard University, Cambridge, Massachusetts 02138, USA*

(Dated: October 16, 2012)

Despite several experiments on chaotic quantum transport, corresponding *ab initio* quantum simulations have been out of reach so far. Here we carry out quantum transport calculations in real space and real time for a two-dimensional stadium cavity that shows chaotic dynamics. Applying a large set of magnetic fields yields a complete picture of the magnetoconductance that indicates fractal scaling on intermediate time scales. Two methods that originate from different fields of physics are used to analyze the scaling exponent and the fractal dimension. They lead to consistent results that, in turn, qualitatively agree with the previous experimental data.

PACS numbers: 05.45.Df, 05.45.Pq, 73.23.Ad, 73.63.Kv

Since the pioneering works of Mandelbrot [1], fractal patterns have been found in a variety of objects in nature including, e.g., snowflakes, fern leaves, coastlines [2, 3], and even music [4–7]. These self-similar (or self-affine) structures were also found in many branches of chemistry and physics; prominent examples are crystal growth and fractal surfaces, and transport in gold nanowires and electron “billiards” [3, 8–11]. In contrast with idealized mathematical fractals continuing to infinitely small scales, fractal scaling in nature has a lower and an upper limit.

While fractals found in nature are often well described by classical theories [1, 3, 8, 9], fractals have also been suggested to manifest in different quantum systems [12–17], where a fundamental lower cutoff for fractal scaling is given by the Heisenberg uncertainty principle. In the case of transport through chaotic systems, such as chaotic electron billiards, both semiclassical (involving quantum interference) and classical mechanisms for the emergence of fractal scaling have been proposed [18, 19].

For quantum systems with an underlying classically *mixed* phase space with both regular and chaotic regions, a quantum graph model suggests a splitting of the chaotic regime into two parts [14]: one part yields fractal conductance fluctuations while the other one leads to isolated resonances on small scales. These isolated resonances were later shown to be associated with the eigenstates of a closed system [20].

A stadium quantum billiard of charged particles is a generic chaotic system, whose underlying classical phase space is chaotic. The phase space becomes mixed in presence of a (perpendicular) magnetic field. In the past two decades the system has been subject to several experiments [10, 21–24]. A typical setup consists of the two-dimensional electron gas (2DEG) in a semiconductor heterostructure, where metallic gates are used to form the geometrical shape of the “billiards” – here called a quantum dot. Alternatively, stadium billiards (and other chaotic systems) can be realized experimentally with mi-

crowave cavities [24].

In this Letter we calculate the fractal scaling of conductance fluctuations in an open *quantum* stadium billiard. Our explicit solution of the time-dependent Schrödinger equation in real space and real time for chaotic transport goes beyond both the semiclassical treatment [18] and the above mentioned quantum graph model [14]. We analyze the fractal scaling using a method which we call minimum-maximum (MIN-MAX) method [3, 10, 25], as well as detrended fluctuation analysis [26–28] (DFA). The MIN-MAX method was used by Sachrajda *et al.* [10] for the analysis of *experimental* magnetoconductance curves. We are able to find a good agreement between theory and experiment, both yielding a fractal dimension $D \sim 1.2 \dots 1.3$.

Model and the computational scheme. – We consider a model for semiconductor stadium device fabricated in the 2DEG of a AlGaAs/GaAs heterostructure similar to Ref. [10]. The Hamiltonian describing our 2D system reads (in atomic units)

$$\hat{H} = \frac{1}{2} [-i\nabla + \mathbf{A}(\mathbf{r})]^2 + V_{\text{ext}}(\mathbf{r}, t), \quad (1)$$

where the vector potential is given in the linear gauge, $\mathbf{A}(\mathbf{r}) = (-By, 0, 0)$, to describe a static and uniform magnetic field perpendicular to the plane. During the time-propagation at $t > 0$, the potential $V_{\text{ext}}(\mathbf{r}, t)$ consists of three parts: (i) a stadium with radius $r = 1$ and width $d = 0.7$, (ii) input and output leads of width $w = 0.56$, and (iii) a linear potential along the propagation direction describing a source-drain voltage. The potential has hard boundaries with a depth $V_0 = 10000$ and the slope of the accelerating linear potential is -100 . The central part of the external potential is shown in Fig. 1. The input and output lead extend further to the left and right.

The *initial* state at $t = 0$ is calculated by taking a small part of the input lead as a potential well. The resulting ground state of a single electron in the well is then used

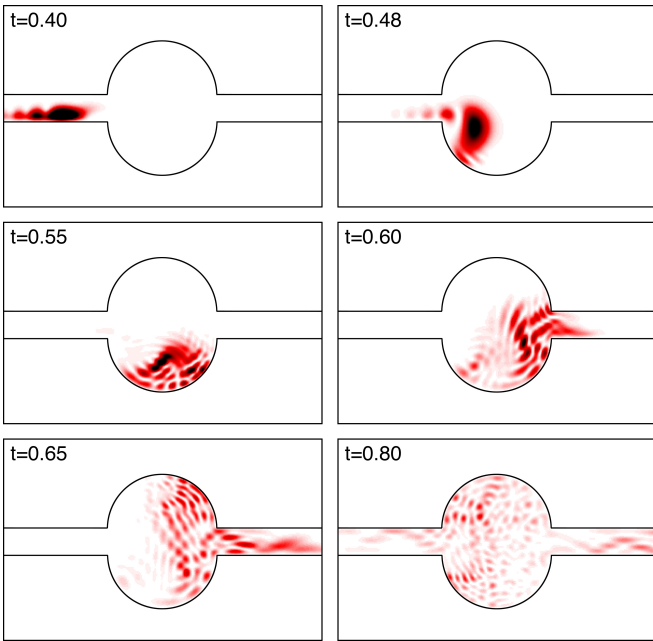


FIG. 1: Snapshots of the electron density in the model stadium system (see text) during a transport simulation with the magnetic flux $\Phi/\Phi_0 = 20$. The input and output leads extend further to the left and right.

as an initial state for the time propagation. At $t > 0$ the above described linear potential accelerates the wave packet across the system. For the time propagation we use a fourth-order Taylor expansion of the time-evolution operator. The **octopus** code package [29] – previously applied for similar real-space transport calculations in quantum rings [30] and Aharonov-Bohm oscillations [31, 32] – is used in all the calculations.

We assess the conductance by calculating the integrated probability density in the output lead from

$$T(\Phi, t) = \int_{\text{output}} d\mathbf{r} |\psi(\Phi, \mathbf{r}, t)|^2, \quad (2)$$

where Φ is the fixed magnetic flux, given above in units of the magnetic flux quantum $\Phi_0 = h/e$. We call T as a transmission coefficient, whose validity in estimating the *relative* conductivity as a function of an external parameter – here the magnetic flux – has been justified in Ref. [30]. Thus, we repeat the time-propagation for different values of Φ to obtain the magnetoconductance that can be compared with the experiments in Ref. [10].

Transport simulations. – In Fig. 1 we show snapshots of the electron density at different times at $\Phi = 20\Phi_0$ through the stadium. Approximately one half of the density is transferred through and other half is either reflected back to the input lead or confined in the stadium. As expected, the density is scattered in the stadium in a chaotic fashion. The size of the wiggles during the scattering depends on the momentum – the higher the

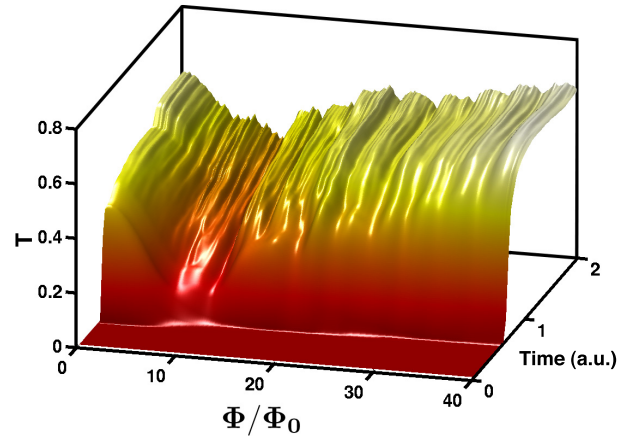


FIG. 2: Transmission coefficient as a function of time and magnetic flux through the stadium.

momentum the higher eigenstates are probed. Here, we have chosen the momentum such that sufficient qualitative complexity is observed, which, as shown below, leads also to a complex behavior of T . On the other hand, the momentum is limited by the grid spacing of the simulation box – all the nodes in the scattered wave packet should be accurately described.

A complete presentation of our transport results is given in Fig. 2, where the transmission coefficient T is plotted as a function of both time and the magnetic flux. The figure consists of 401 respective time-propagations, each with a fixed number of flux quanta Φ/Φ_0 ranging from zero to 40 in steps of 0.1. The flux range is qualitatively similar to the experiment in Ref. [10]. A complex magnetoconductance is formed if the propagation time is larger than ~ 1 . A cross section of the conductance at $t = 1.4$ is shown in Fig. 3. We point out that due to the finite system size we are not able to reach the *equilibrium* current and thus find the absolute conductance. Therefore, we consider fixed propagation times through the parameter range of Φ/Φ_0 . In other words, a fixed propagation time is expected to treat all the values of Φ/Φ_0 equally in order to obtain the relative conductance T .

Now, the essential question is after which times fractals are found, and how the fractal dimension changes over time. This is analyzed in the following with two techniques: the MIN-MAX method [3, 10, 25], and DFA [26–28].

Minimum-maximum method. – To extract the fractal dimension D for a mapping $f : \mathbb{R} \rightarrow \mathbb{R}$, the domain of the given function is first divided into length intervals Δx . The difference between the minimum and maximum of the function is calculated within every interval and added up. In case of fractal scaling, the resulting sum is

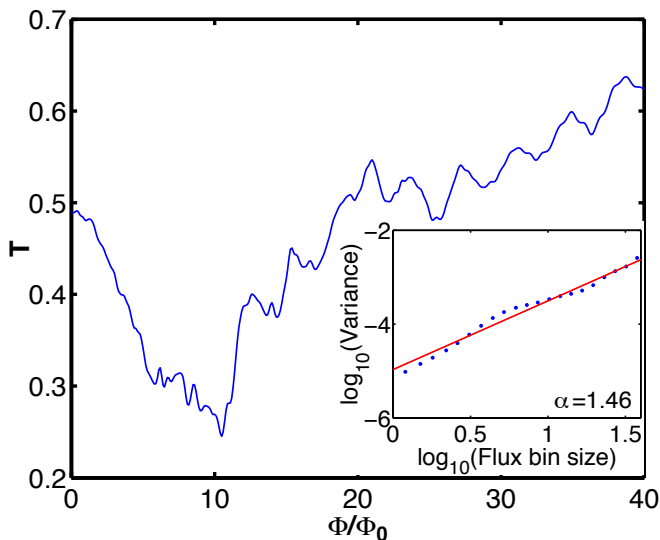


FIG. 3: Transmission coefficient as a function of the magnetic flux at $t = 1.4$. The inset shows the scaling exponent $\alpha = 1.46$ obtained from the DFA analysis.

a power-law function of the interval length [3, 10, 25]:

$$\sum_i [\max f(x) - \min f(x)]_{|x-x_i| < \Delta x/2} = \lambda(\Delta x)^{-D+1}. \quad (3)$$

Detrended fluctuation analysis.— DFA is a standard method that was developed in the context of time-series analysis [26] and has proven to be very reliable particularly in dealing with non-stationary time-series and trends in the data [6, 26, 27, 33, 34]. It has also been used outside the time domain, e.g., to study the organization of DNA nucleotides [28]. However, to our knowledge, DFA has not been applied to fractal conductance curves before.

The standard procedure of DFA consists of the following four steps [26, 27]: (1) integrating the time series, (2) dividing the series into windows of size s , (3) fitting with a polynomial $f_s(i)$ of degree $m = 2 \dots 4$ that represents the trend in the window, and (4) calculating the variance with respect to the local trend $f_s(i)$ from

$$\begin{aligned} F(s) &= \langle (f(i) - f_s(i))^2 \rangle \\ &= \frac{1}{N-1} \sum_{i=1}^N (f(i) - f_s(i))^2 \sim s^\alpha. \end{aligned} \quad (4)$$

The key point in applying DFA to study conductance fluctuations is to relate the exponent α to the quantity of interest (here: the fractal dimension D). It is known that $D = 2 - \gamma/2$ with $\langle (\Delta G)^2 \rangle \sim (\Delta B)^\gamma$ [10, 18]. The latter is exactly step (4) of the DFA analysis above. We therefore omit step (1) and identify $\alpha = \gamma$, hence the fractal dimension reads $D = 2 - \alpha/2$.

Results.— In DFA, we apply quadratic detrending ($m = 2$) to our data in Fig. 3. The inset shows the

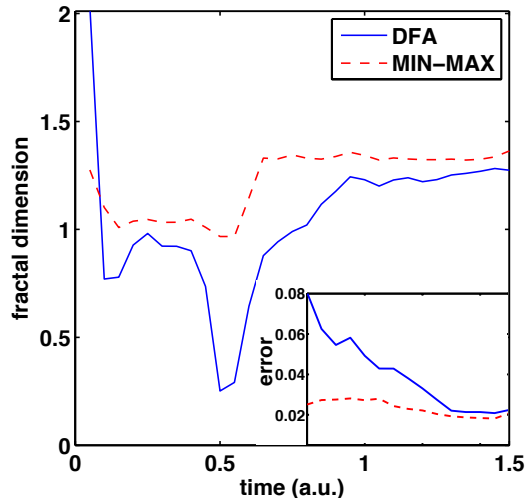


FIG. 4: Fractal dimension D calculated from DFA with the relation $D = 2 - \alpha/2$ and from the MIN-MAX method, respectively, during the time-propagation. Note that the fractal structure is developed only at $t \gtrsim 1$. The inset shows the time-development of the error in the fitting procedure at $t = 0.8 \dots 1.5$ (see text).

fitting of the data (solid line) at $t = 1.4$ that yields $\alpha = 1.46$. This qualitatively agrees well with the experimental result $\gamma = \alpha = 1.38$ of Sachrajda *et al.* [10]. The corresponding fractal dimension extracted from DFA is $D = 1.27$. In comparison, the MIN-MAX method yields $D = 1.32$ for our data, whereas the corresponding experimental result – obtained with the same method – is $D = 1.25$ [10]. Concluding, we find an excellent agreement of the results both regarding the different methods and comparison with the experimental data. We point out that our stadium model is similar to the experiment and the channel dimensions are also comparable. According to our calculations, increasing the channel width from 0.56 to 0.7 leads to the same D obtained in the MIN-MAX method, whereas DFA yields a slightly smaller D .

In Fig. 4 we show the time-development of the fractal dimension obtained from DFA and the MIN-MAX method, respectively. We point out that at times $t \lesssim 0.5$ the quality of the fitting is poor – or the fitting is ill-defined *per se* – as the conductance curve as a function of the flux has not yet been developed (see Fig. 2). Secondly, the clear signatures of a fractal structure are developed only at $t \gtrsim 1$. Nevertheless, D converges during the time-propagation towards the values given above, and the quality of the fitting in both methods improves as well. The inset in Fig. 4 shows the error in the fitting, $\text{ERR} = 1 - \text{CC}^2$, for times $t = 0.8 \dots 1.5$. Here CC is the Pearson product-moment correlation coefficient of the log-log data. Thus, ERR measures the linear fit quality such that $\text{ERR} = 0$ corresponds to exact linear behavior. The minimum of the error is obtained at $t \approx 1.4$,

which is the optimal time used above to determine α and D . At larger times with $1.45 \lesssim t < 1.5$, we find a small bump in D in Fig. 4 corresponding to an upward kink in the error in the inset. This is the first signature of back-scattering effects due to the finite simulation box (see above). In this way we are able to determine the range of validity in our scheme to determine the fractal dimension.

In summary, we have calculated the time-evolution of a single-electron wave packet through a two-dimensional stadium-shaped cavity by solving the Schrödinger equation in real time and real space. The relative conductance has been calculated for a large set of magnetic fluxes in order to analyze the fractal nature of the magnetoconductance. We have found that the conductance shows clear indications for fractal scaling. The fractal dimensions extracted from two respective methods are consistent with each other. Moreover, we have found an excellent qualitative agreement with previous experimental results. Our findings indicate that DFA suits well for the analysis of fractal scaling in chaotic quantum transport. Hence, we suggest to extend the use of the concept of data detrending (and hence DFA) to study fractal scaling of transport and other characteristics in chaotic (quantum) systems.

This work was supported by the Magnus Ehrnrooth Foundation, Wihuri Foundation, and the Academy of Finland. HH acknowledges funding through the German Research Foundation (DFG, grant no. 6312/1-2). CSC Scientific Computing Ltd is acknowledged for computational resources.

* Electronic address: esa.rasanen@tut.fi

- [1] B. B. Mandelbrot, *The Fractal Geometry of Nature* - Benoit B. Mandelbrot - Google Books (1983).
- [2] B. Mandelbrot, *Science* **156**, 636 (1967).
- [3] P. Meakin, Cambridge University Press (1998).
- [4] R. Viss and J. Clarke, *Nature* **258**, 317 (1975).
- [5] K. J. Hsu and A. J. Hsu, *Proc. Nat. Acad. Sci.* **87**, 938 (1990).
- [6] H. Hennig, R. Fleischmann, A. Fradebohm, Y. Hagemayer, J. Nagler, A. Witt, F. J. Theis, and T. Geisel, *PLoS ONE* **6**, e26457 (2011).
- [7] H. Hennig, R. Fleischmann, and T. Geisel, *Physics Today* **65**, 64 (2012).
- [8] T. Michely and J. Krug, *Islands, Mounds, and Atoms, Patterns and Processes in Crystal Growth Far from Equilibrium* (Springer Verlag, 2004).
- [9] M. F. Barnsley and Mathematics, *Fractals Everywhere* (2012).
- [10] A. Sachrajda, R. Ketzmerick, C. Gould, and Y. Feng, *Phys. Rev. Lett.* **80**, 1948 (1998).
- [11] H. Hegger, B. Huckestein, K. Hecker, M. Janssen, A. Freimuth, G. Reckziegel, and R. Tuzinski, *Phys. Rev. Lett.* **77**, 3885 (1996).
- [12] M. V. Berry, *J. Phys. A* **29**, 6617 (1996).
- [13] D. Wójcik, I. Białynicki-Birula, and K. Życzkowski, *Phys. Rev. Lett.* **85**, 5022 (2000).
- [14] L. Hufnagel, R. Ketzmerick, and M. Weiss, *Europhysics Letters* **54**, 703 (2001).
- [15] G. Benenti, G. Casati, I. Guarneri, and M. Terraneo, *Phys. Rev. Lett.* **87**, 6209 (2001).
- [16] I. Guarneri and M. Terraneo, *Phys. Rev. E* **65**, 4 (2001).
- [17] E. Louis and J. Vergés, *Phys Rev B* (2000).
- [18] R. Ketzmerick, *Phys Rev B* **54**, 10841 (1996).
- [19] H. Hennig, R. Fleischmann, L. Hufnagel, and T. Geisel, *Phys. Rev. E* **76**, 015202(R) (2007).
- [20] A. Bäcker, A. Manze, B. Huckestein, and R. Ketzmerick, *Phys. Rev. E* **66**, 016211 (2002).
- [21] C. Marcus, A. Rimberg, R. Westervelt, and P. Hopkins, *Phys. Rev. Lett.* **69**, 506 (1992).
- [22] A. Micolich, R. Taylor, A. Davies, and J. Bird, *Phys. Rev. Lett.* **87**, 036802 (2001).
- [23] Y. Takagaki, M. ElHassan, A. Shailos, and C. Prasad, *Phys Rev B* **62**, 10255 (2000).
- [24] U. Kuhl, H.-J. Stöckmann, and R. Weaver, *J. Phys. A* **38**, 10433 (2005).
- [25] B. Dubuc, J. F. Quiniou, C. Roques-Carnes, C. Tricot, and S. W. Zucker, *Phys. Rev. A* **39**, 1500 (1989).
- [26] C. K. Peng, S. Havlin, H. E. Stanley, and A. L. Goldberger, *Chaos* **5**, 82 (1995).
- [27] J. Kantelhardt, E. Koscielny-Bunde, H. Rego, S. Havlin, and A. Bunde, *Physica A* **295**, 441 (2001).
- [28] C.-K. Peng, S. V. Buldyrev, S. Havlin, M. Simons, H. E. Stanley, and A. L. Goldberger, *Phys. Rev. E* **49**, 1685 (1994).
- [29] M. A. L. Marques, A. Castro, G. F. Bertsch, A. Rubio, *Comput. Phys. Commun.* **151**, 60 (2003); A. Castro, H. Appel, M. Oliveira, C. A. Rozzi, X. Andrade, F. Lorenzen, M. A. L. Marques, E. K. U. Gross, and A. Rubio, *Phys. Stat. Sol. (b)* **243**, 2465 (2006).
- [30] V. Kotimäki and E. Räsänen, *Phys. Rev. B* **81**, 245316 (2010).
- [31] V. Kotimäki, E. Cicek, A. Siddiki, and E. Räsänen, *New J. Phys.* **14**, 053024 (2012).
- [32] A. Salman, V. Kotimäki, A. Siddiki, and E. Räsänen, *arXiv:1210.3134*.
- [33] H. D. Jennings, P. C. Ivanov, A. M. Martins, P. C. Silva, and G. M. Viswanathan, *Physica A* **336**, 585 (2004).
- [34] P. C. Ivanov, Q. Ma, R. P. Bartsch, J. M. Hausdorff, L. A. N. Amaral, V. Schulte-Frohlinde, H. E. Stanley, and M. Yoneyama, *Phys. Rev. E* **79**, 1 (2009).